Wide angle SAR imaging method based on Hybrid Representation

Yao Zhao,[1] Yanxu Chen,[1] He Tian,[2,3] Xiangyin Quan,[4] Bingo Wing-Kuen Ling,[1] and Zhe Zhang ✉ [5,6,7]

[1]*Guangdong University of Technology , Guangzhou 510006, China*
[2]*National key laboratory of scattering and radiation, Beijing, 100854, China*
[3]*Beijing Institute of Environment Features, Beijing, 100854, China*
[4]*China Academy of Launch Vehicle Technology, Beijing 100076, China*
[5]*Suzhou Key Laboratory of Microwave Imaging, Processing and Application Technology, Suzhou 215000, China*
[6]*Suzhou Aerospace Information Research Institute, Suzhou 215000, China*
[7]*Aerospace Information Research Institute, Chinese Academy of Sciences, Beijing 100190, China*
Correspondence: Zhe Zhang, zhangzhe01@aircas.ac.cn

In this paper, we investigate the application of Hybrid Representation in Wide-Angle Synthetic Aperture Radar (WASAR) imaging, addressing the challenges of achieving sparse representation in the presence of complex electromagnetic scattering characteristics and highly anisotropic targets. We utilize a Convolutional Neural Network (CNN) to represent two-dimensional data within the same subaperture, while employing dictionary learning for sparse representation across different subapertures. Convolutional Neural Networks (CNNs) excel at learning spatial hierarchies and local dependencies in two-dimensional data, but require a large amount of training data. Isotropic targets within subapertures can be used for training with conventional SAR data, whereas anisotropic targets present challenges in obtaining training samples. To address this, a dictionary for different subapertures is generated from measurements using dictionary learning, eliminating the need for additional training data. By integrating these methods, we propose a novel approach, Hybrid-WASAR, which incorporates two regularization terms into WASAR imaging and employs the Alternating Direction Method of Multipliers (ADMM) to iteratively solve the imaging model. Compared to traditional WASAR imaging techniques, Hybrid-WASAR not only enhances the accuracy of the reconstructed target backscatter coefficients, but also effectively reduces sidelobes and noise, resulting in a significant improvement in overall imaging quality.

Introduction: Wide-Angle Synthetic Aperture Radar (WASAR) acquires echo signals from targets over an extensive azimuth angle, resulting in higher azimuth resolution compared to conventional SAR [1]. WASAR images facilitate the extraction of backscattering anisotropy characteristics of targets, which possess significant application value in target identification and classification domains [2]. By integrating sparse signal processing with WASAR, researchers have made substantial progress in addressing the underdetermined inverse problem associated with anisotropic targets [3]. Sparse signal processing relies on the assumption that targets are sparse or can be sparsely represented within a specific dictionary [4]. However, typical radar observation scenes are not sparse, and achieving effective sparse characterization of targets remains a challenge. This issue becomes more complex when dealing with anisotropic targets.

There are two strategies for sparsely representing anisotropic targets: within a single subaperture or across multiple subapertures. For sparse representation within a single subaperture, several approaches can be employed. These include utilizing fixed dictionaries, such as wavelet transform [5] and curvelet transform [6]; applying sparse dictionary learning [7]; or leveraging deep learning [8] to obtain target representations. For sparse representation across multiple subapertures, various dictionary construction methods are available. These include methods based on parametric models, such as scattering theory model approaches [9] and typical shape feature models [10]. Additionally, dictionaries can be constructed using fixed dictionaries, exemplified by orthogonal dictionaries [11], rectangular, or Gaussian functions [12]. While predefined sparse representations have limitations and depend on human design, deep learning methods can potentially provide more effective representations. However, they come with their own set of challenges, such as the need for large amounts of data and computational resources.

In this letter, we present a WASAR imaging method based on a hybrid sparse representation of anisotropic targets. The sparse representation involves representing 3D data as a 2D image sparse representation within each subaperture, while the representation across different subapertures constitutes the third dimension. Convolutional Neural Networks (CNNs) [13] are employed for representation within a single subaperture, while dictionary learning [14] is utilized for representation across multiple subapertures. CNNs excel at uncovering spatial feature hierarchies and recognizing local dependencies in data, making them particularly suitable for representing two-dimensional data within a single subaperture. The CNN representation methods remain applicable, as targets exhibit isotropic properties within an individual subaperture. Owing to the complexity of electromagnetic scattering from anisotropic targets, their representation across different subapertures is achieved using dictionary learning. Fixed dictionaries often fall short in producing satisfactory results, and deep learning methods that rely on large datasets of anisotropic targets frequently lack sufficient training data. The dictionary learning in this method relies on measurement data and does not require external training data. This allows the WASAR imaging algorithm to strike a balance between reconstruction performance and training sample requirements. It is important to emphasize that, in this letter, dictionary learning and target sparse coefficient reconstruction are performed simultaneously.

To achieve accurate reconstruction, this paper establishes a regularized optimization model incorporating two regularization constraints: one to constrain the sparse representation based on CNNs within the same subaperture, and the other to sparsely represent anisotropic objectives across different subapertures using the dictionary learning approach. We employ the Alternating Direction Method of Multipliers (ADMM) to solve the model, breaking down the optimization problem into manageable subproblems, updating each parameter sequentially, and ultimately obtaining the WASAR imaging results..

Signal Model: For wide-angle SAR, the backscattering coefficient is related not only to the spatial position of the target, but also to the radar azimuth angle, denoted as $x\,(p_r, q_r, \theta) = x\,(r, \theta)$ where p_r and q_r denote the fast time and slow time positions of the target r, θ is azimuth incident angle. The scattering function of WASAR in matrix representation can be expressed as follows,

$$\mathcal{X}_{L\times K} = \begin{pmatrix} x(r_1,\theta_1) & x(r_1,\theta_2) & \cdots & x(r_1,\theta_K) \\ x(r_2,\theta_1) & x(r_2,\theta_2) & \cdots & x(r_2,\theta_K) \\ \vdots & \vdots & \ddots & \vdots \\ x(r_L,\theta_1) & x(r_L,\theta_2) & \cdots & x(r_L,\theta_K) \end{pmatrix} \tag{1}$$

where L is the number of pixels in the image and K is the number of subapertures in WASAR. Each row of the matrix represents the imaging of the target across all subapertures, while each column of the matrix represents the individual imaging results of a subaperture in WASAR.

The baseband form of echo signal y can be expressed as,

$$y = \mathcal{R}(\mathcal{X}) + z, \tag{2}$$

where $\mathcal{R}$ denotes the measurement operator for WASAR imaging and z is the noise.

Convolutional Neural Networks (CNNs) are a type of deep learning architecture specifically designed for image processing and analysis. They excel at approximating and representing image data by learning spatial hierarchies and local patterns. In image reconstruction tasks, a learned CNN, denoted as $\mathcal{D}_w$, is used to approximate the image x after removing alias artifacts and noise. A separate learned CNN estimator of noise and alias patterns, denoted as $\mathcal{N}w$, depends on the learned parameters w. We can express $\mathcal{N}w$ as the difference between the input image x and the image reconstructed by $\mathcal{D}_w$:

$$\mathcal{N}_w(\mathcal{X}) = (\mathcal{I} - \mathcal{D}_w)(\mathcal{X}) = \mathcal{X} - \mathcal{D}_w(\mathcal{X}). \tag{3}$$

The CNN-based prior, which is given by $|\mathcal{N}_w(\mathcal{X})|^2$, assigns high values when the image is contaminated with noise and alias patterns.

Represent $\mathcal{X}_{L\times K}$ as the product of a sparse coefficient matrix $\mathrm{U}_{L\times T}$

and a dictionary matrix $V_{T\times K}$, composed of temporal basis functions,

$$\underbrace{\begin{pmatrix} x(r_1,\theta_1) & x(r_1,\theta_2) & \cdots & x(r_1,\theta_K) \\ x(r_2,\theta_1) & x(r_2,\theta_2) & \cdots & x(r_2,\theta_K) \\ \vdots & \vdots & \ddots & \vdots \\ x(r_L,\theta_1) & x(r_L,\theta_2) & \cdots & x(r_L,\theta_K) \end{pmatrix}}_{X_{L\times K}} = \underbrace{\begin{pmatrix} u_1(r_1) & \cdots & u_T(r_1) \\ u_1(r_2) & \cdots & u_T(r_2) \\ \vdots & \ddots & \vdots \\ u_1(r_L) & \cdots & u_T(r_L) \end{pmatrix}}_{U_{L\times T}} \cdot \underbrace{\begin{pmatrix} v_1(\theta_1) & \cdots & v_1(\theta_K) \\ v_2(\theta_1) & \cdots & v_2(\theta_K) \\ \vdots & \ddots & \vdots \\ v_T(\theta_1) & \cdots & v_T(\theta_K) \end{pmatrix}}_{V_{T\times K}} \cdot \tag{4}$$

where T denotes the total number of basis functions present in the dictionary. The sparse representation of (4) can also be expressed as

$$x(r,\theta) = \sum_{t=1}^{T} u_t(r) v_t(\theta) \tag{5}$$

where $u_t(r)$ represents the t-th column of U, which corresponds to the t-th spatial weight, $v_t(\theta)$ represents the t-th row of V, corresponding to the t-th temporal basis function. Sparsity constraints are imposed on the rows of U. As a result, the number of non-zero entries is greatly reduced, indicating that only a small subset of the temporal basis functions is needed to model the temporal profile at each voxel. Our over-complete dictionary of basis functions is estimated directly from the data and may not necessarily be orthogonal. Figure 1 shows the diagram of the hybrid representation of anisotropic targets in WASAR.

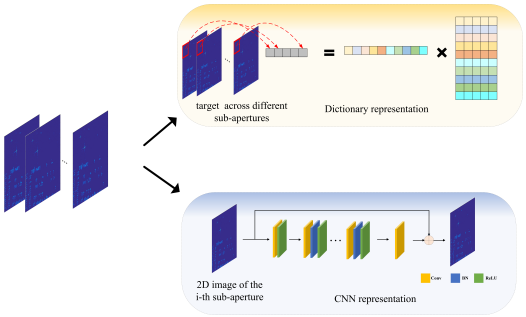

Fig 1 *Hybrid representation of anisotropic targets in WASAR.*

WASAR imaging method: In the context of the BCS model specified by (3) and (4), our focus is on recovering the scattering function $\mathcal{X}$. To accomplish this, we adopt two regularization terms: one for the CNN representation within the subaperture and one for the dictionary representation across subapertures. Specifically, we cast the joint estimation of U and V from the measurements as a constrained optimization problem. The CNN used in our approach is a pre-trained network.

$$\begin{aligned} \mathcal{X}^* = U^*V^* = \arg\min_{U,V} \|\mathcal{R}(UV) - y\|_F^2 + \lambda_1\|U\|_1 \\ +\lambda_2\|\mathcal{N}_w(|UV|)\|^2 s.t.\ \|V\|_F^2 \le 1 \end{aligned} \tag{6}$$

where $\|\mathcal{R}(UV) - y\|_F^2$ ensures data consistency. $\|U\|_{l_1}$ is l_1 norm of U to characterize U's sparsity. This penalty term can impose a sparse prior constraint to WASAR images across different subaperture. A unit Frobenius norm $\|V\|_F^2$ is then imposed on V , which serves to making the recovery problem well posed. $\|\mathcal{N}_w(|UV|)\|^2$ can be thought of as a pre-trained CNN denoiser, used to represent the isotropic targets in the same subaperture image. λ_1 and λ_2 denotes the regularization parameter of the WASAR imaging model. By leveraging the Augmented Lagrangian (AL) framework, we can convert the optimization problem in (6) into the following form,

$$\begin{aligned} \ell(U,V,L,Q,\mathcal{X}) = \|\mathcal{R}(\mathcal{X}) - y\|_F^2 + \frac{\beta_\mathcal{X}}{2}\|\mathcal{X} - UV\|_F^2 \\ +\Lambda_\mathcal{X}(\mathcal{X} - UV) + \frac{\lambda_1\beta_U}{2}\|U - L\|_F^2 + \frac{\beta_V}{2}\|V - Q\|_F^2 \\ +\Lambda_V(V - Q) + \lambda_1\|L\|_1 + \lambda_2\|\mathcal{N}_w(\mathcal{X})\|^2 s.t.\ \|Q\|_F^2 < 1 \end{aligned} \tag{7}$$

where Q , L is the auxiliary variable, Λ_V , $\Lambda_\mathcal{X}$ is the Lagrange multiplier, and β_V , β_U , $\beta_\mathcal{X}$ is the penalty parameter.

We use the ADMM algorithm for solving (7) , which can be optimized by alternating the five variables U , V , L , Q , $\mathcal{X}$ for updating.

$$\arg\min_{L} \frac{\lambda\beta_U}{2}\|U - L\|_F^2 + \lambda\|L\|_{l_p} \tag{8}$$

$$\arg\min_{U} \frac{\beta_\mathcal{X}}{2}\|\Gamma - UV\|_F^2 + \Lambda_\mathcal{X}(\mathcal{X} - UV) + \frac{\lambda\beta_U}{2}\|U - L\|_F^2 \tag{9}$$

$$\arg\min_{Q} \frac{\beta_V}{2}\|V - Q\|_F^2 + \Lambda_\mathcal{X}(\mathcal{X} - UV) s.t.\ \|Q\|_F^2 < 1 \tag{10}$$

$$\begin{aligned} \arg\min_{V} \frac{\beta_\mathcal{X}}{2}\|\mathcal{X} - UV\|_F^2 + \Lambda_\mathcal{X}(\mathcal{X} - UV) + \frac{\beta_V}{2}\|V - Q\|_F^2 \\ +\Lambda_V(V - Q) \end{aligned} \tag{11}$$

$$\begin{aligned} \arg\min_{\mathcal{X}} \|\mathcal{R}\mathcal{X} - y\|_F^2 + \frac{\beta_\mathcal{X}}{2}\|\mathcal{X} - UV\|_F^2 + \Lambda_\mathcal{X}(\mathcal{X} - UV) \\ +\lambda_2\|\mathcal{N}_w(|\mathcal{X}|)\|^2 \end{aligned} \tag{12}$$

At each iteration, we use a steepest ascent method to update all the Lagrange multipliers, as follows,

$$\Lambda_{V_{(n+1)}} = \Lambda_{V_n} + \beta_V(V_{n+1} - Q_{n+1}) \tag{13}$$

$$\Lambda_{\mathcal{X}_{(n+1)}} = \Lambda_{\mathcal{X}_n} + \beta_\mathcal{X}(\mathcal{X}_{n+1} - U_{n+1}V_{n+1}). \tag{14}$$

The similar solution of these five subprobles can be obtained in [15]. The solution for Eq. (8), Eq. (11) and Eq. (12) can be obtained by shrinkage rule. Eq. (9) and Eq. (10) is a quadratic subproblem, which yields closed form solution.

Experiments and analysis of results: To demonstrate the effectiveness of the proposed algorithm in reconstructing the backscattering coefficients of anisotropic targets, we conducted simulations and experiments. In both instances, we divided each subaperture into 1 degree increments, selecting a total of 20 subapertures. In the simulation designed to evaluate the proposed method, we employed the sinc function to characterize the aspect dependence of anisotropic objects. In the experiments, we utilized data from the Gotcha dataset [16], which features a target scenario of a parking lot filled with numerous cars. The Convolutional Neural Network (CNN) used in Hybrid-WASAR is pre-trained in a manner similar to the approach described in [8]. We set the number of basis functions in dictionary learning to 40. We compared the performance of Hybrid-WASAR with the backward projection (BP) algorithm [17] and the CS algorithm [18] to evaluate its effectiveness.

Figure 2 presents the subaperture reconstruction simulation results for anisotropic targets using the BP, CS, and Hybrid-WASAR algorithms. All three methods demonstrate accurate reconstruction capabilities. However, Hybrid-WASAR outperforms the BP and CS algorithms in reconstructing the subaperture corresponding to the target's maximum response amplitude, where the latter two exhibit minor deviations. As the scattering amplitude gradually decreases, the BP and CS algorithms produce larger deviations, while Hybrid-WASAR continues to deliver superior reconstruction results. This closely aligns with the true sinc function curve, ultimately generating a more accurate image.

Figure 3 shows the subaperture and full-aperture reconstruction results of the Gotcha dataset using the BP, CS, and Hybrid-WASAR algorithms. In the subaperture results, the BP algorithm yields the poorest performance, exhibiting numerous sidelobes and noise, which hinder effective target distinction. In contrast, both the CS and Hybrid-WASAR algorithms display substantially fewer sidelobes. The target edges are more clearly and sharply depicted with Hybrid-WASAR, especially in the lower left section of the image, where the proposed method demonstrates enhanced distinguishability. Subsequently, we generate full-aperture images from the subaperture images. The Hybrid-WASAR algorithm noticeably reduces the sidelobes of the strong point target

compared to BP and CS. Moreover, the car within the red box in the figure is better imaged by the proposed method. Figures 3(d), 3(e), and 3(f) highlight two rows of cars framed in red, while Figure 4 provides a magnified view of these vehicles. Table 1 presents the target background ratio (TBR) and entropy of the WASAR imaging results, revealing that the proposed algorithm outperforms the other methods in both TBR and entropy. This demonstrates the superior reconstruction capabilities of the proposed method.

Conclusion: In this paper, we introduced the application of Hybrid Representation to WASAR, resulting in the novel Hybrid-WASAR imaging method. The proposed method employs CNN representation for subaperture images, taking advantage of the training sample set for isotropic targets within subapertures. Simultaneously, dictionary learning for anisotropic targets across different subapertures eliminates the need for additional training data. This approach achieves an optimal balance between training sample requirements and reconstruction performance. By utilizing the ADMM method, Hybrid-WASAR decomposes the optimization problem into individual sub-problems and iteratively solves each one to obtain optimal results. When compared to the BP and CS algorithms, Hybrid-WASAR delivers superior imaging quality for anisotropic targets. Both simulation and real-data experiment results demonstrate that Hybrid-WASAR provides enhanced reconstruction accuracy, as well as improved sidelobe suppression and noise reduction capabilities.

Acknowledgments: This research was funded in part by The Natural Science Foundation of Guangdong Province (2021A1515012009).

Table 1. The TBR and entropy of the Gotcha dataset

	BP	CS	Hybrid-WASAR
TBR(dB)	25.84	32.25	**36.19**
Entropy	5.52	5.36	**5.27**

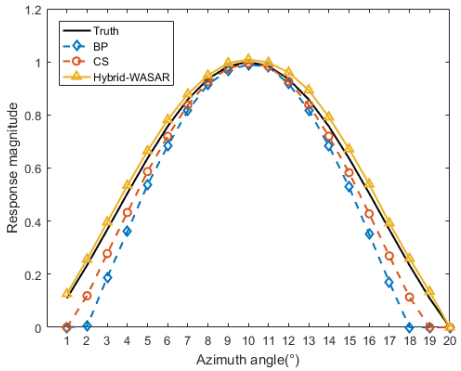

Fig 2 *Reconstruction result of anisotropic target over all the subapertures.*

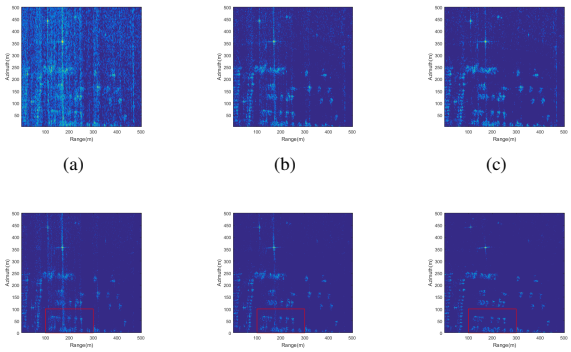

Fig 3 *The subaperture and full aperture imaging results of X-band data. (a) 1st subaperture image generated by BP. (b) 1st subaperture image generated by CS.(c) 1st subaperture image generated by Hybrid-WASAR. (d) The full aperture image generated by BP. (e) The full aperture image generated by CS.(f) The full aperture image generated by Hybrid-WASAR.*

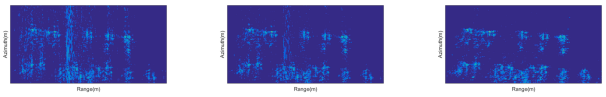

Fig 4 *The zoomed-in results of full-apertures images. (a) BP. (b) CS.(c) Hybrid-WASAR.*

References

1. Moses R L, C.M. Potter L C: Wide-angle sar imaging. In Algorithms for Synthetic Aperture Radar Imagery XI 5427, 164–175 (2004)
2. Wang X, C.C. Chang G: Enhanced anisotropic scattering targets imaging in wide-angle sar. Progress In Electromagnetics Research C 107, 127–141 (2021)
3. Wei Z, W.Y. Zhang B: Accurate wide angle sar imaging based on ls-cs-residual. Sensors 19(3), 490 (2019)
4. Varshney K R, F.J.W. Çetin M: Sparse representation in structured dictionaries with application to synthetic aperture radar. IEEE Transactions on Signal Processing 56(8), 3548–3561 (2008)
5. G, A.: A new statistical-based kurtosis wavelet energy feature for texture recognition of sar images. IEEE Transactions on Geoscience and Remote Sensing 50(11), 4358–4368 (2012)
6. Zhou H, C.P.: Oil spill identification in sar image using curvelet transform and svm. In 2019 International Conference on Intelligent Transportation, Big Data and Smart City (ICITBS) pp. 574–577. (2019)
7. Shi M, L.X. Gao Y: Multi-structure extraction kernel dictionary learning for sar target recognition. In IGARSS 2022-2022 IEEE International Geoscience and Remote Sensing Symposium pp. 2638–2641. (2022)
8. Alver M B, C.M. Saleem A: Plug-and-play synthetic aperture radar image formation using deep priors. IEEE Transactions on Computational Imaging 7, 43–57 (2020)
9. Gerry M J, G.I.J. Potter L C: A parametric model for synthetic aperture radar measurements. IEEE transactions on antennas and propagation 47(7), 1179–1188 (1999)
10. Saville M A, F.D.F. Jackson J A: Rethinking vehicle classification with wide-angle polarimetric sar. IEEE Aerospace and Electronic Systems Magazine 29(1), 41–49 (2014)
11. Gao Y, G.L. Xing M: Extraction of anisotropic characteristics of scattering centers and feature enhancement in wide-angle sar imagery based on the iterative re-weighted tikhonov regularization. Remote Sensing 10(12), 2066 (2018)
12. Cong X, L.X. Gui G: Object-level sar imaging method with canonical scattering characterisation and inter-subdictionary interferences mitigation. IET Radar, Sonar and Navigation 10(4), 784–790 (2016)
13. Zhang K, G.S. Zuo W: Learning deep cnn denoiser prior for image restoration. In Proceedings of the IEEE conference on computer vision and pattern recognition pp. 3929–3938. (2017)
14. Rubinstein R, E.M. Bruckstein A M: Dictionaries for sparse representation modeling. Proceedings of the IEEE 98(6), 1045–1057 (2010)
15. Bhave S, J.M. Lingala S G: A variable splitting based algorithm for fast multi-coil blind compressed sensing mri reconstruction. In 2014 36th Annual International Conference of the IEEE Engineering in Medicine and Biology Society pp. 2400–2403. (2014)
16. Casteel Jr C H, M.M.J. Gorham L R A: A challenge problem for 2d/3d imaging of targets from a volumetric data set in an urban environment. In Algorithms for Synthetic Aperture Radar Imagery XIV 6568, 97–103 (2007)
17. Moses, R.L., Ash, J.N.: An autoregressive formulation for sar backprojection imaging. IEEE Transactions on Aerospace and Electronic Systems 47(4), 2860–2873 (2011)
18. Wei Z, W.Z. Yang L: Wide angle sar subaperture imaging based on modified compressive sensing. IEEE Sensors Journal 18(13), 5439–5444 (2018)